5. PORE-WATER PRESSURE IN EMBANKMENT

5.1 Pore-Water Pressure Built-up during Construction

Hilf proposed a method of estimating built-up pore-water pressure during construction, where the increase of pore-water pressure Δu due to the increase in total stress applied under undrained condition is given by the following formula:

$$\Delta u = p_0 \frac{\delta}{(v_a + H_e v_w) - \delta} \qquad \text{..... (5.1)}$$

in which v_a and v_w are, respectively, air and water content in unit volume of soil, δ is the amount of volume compression, and H_e and p_0 are Henry's coefficient of solubility (usually $H_e = 0.02$) and the atmospheric pressure. Eq.(5.1) is considered valid only if the degree of saturation of soil is higher than 85%.

Another method of estimation can be provided by the direct measurement of pore-water pressure in laboratory compression tests performed on compacted soils under undrained condition. The results obtained by both methods are compared in Fig.5.1.

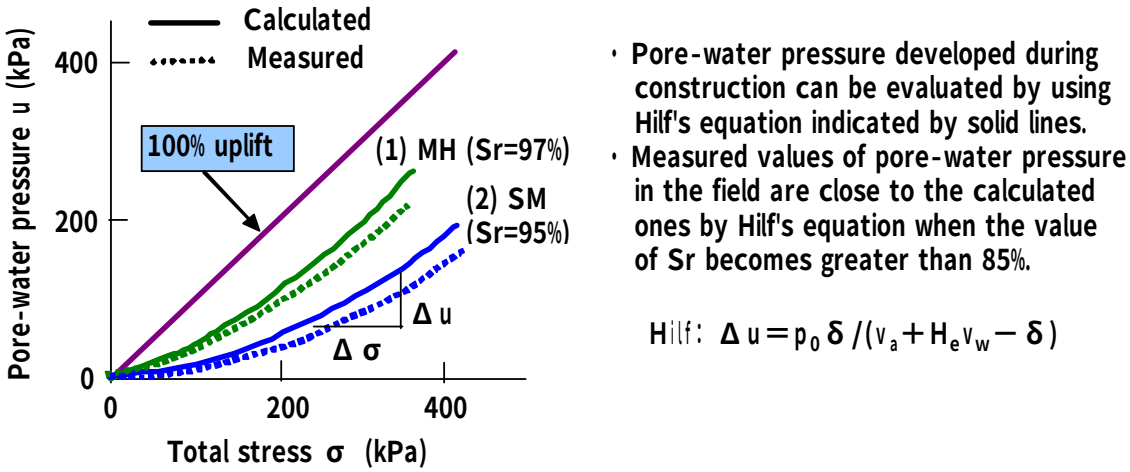

Fig.5.1 Estimation of Built-up Pore-Water Pressure

5.2 Dissipation of Pore-Water Pressure

Pore-water pressure estimated by Eq.(5.1) is the one developed when the total stress is applied under a completely undrained condition. In an embankment dam, however, some part of this built-up pore-water pressure should be dissipated during construction. Though the Terzaghi's theoretical equation of consolidation is valid to evaluate the amount of dissipation, it is not practical for actual dams because of their complicated boundary and discontinuity conditions in the section.

A practically useful method of estimating pore-water pressure during construction is presented in Fig.5.2. Consider that variation of the observed pore-water pressure u is drawn with time for a typical soil element in an embankment. The degree of consolidation (or the rate of

dissipation) U of this element up to the time $t=\Delta t$ is defined by $U=(u_H-u)/u_H$, where u_H is obtained from the Hilf's equation or by experiment as noted before. On the other hand, the elapsed time t can be expressed in a dimensionless form, with the coefficient of consolidation c_v of fill materials and the drainage distance H between the drain and the point under consideration, in terms of the time factor as $T=c_vt/H^2$. By making use of much available data on the observed pore-water pressure, relations between U and T are obtained for several types of embankment. In Fig.5.2(b), mean U-T relation curves are given for four different typical types of embankment dam. Also presented by a dashed curve is the Terzaghi's theoretical solution of one-dimensional consolidation.

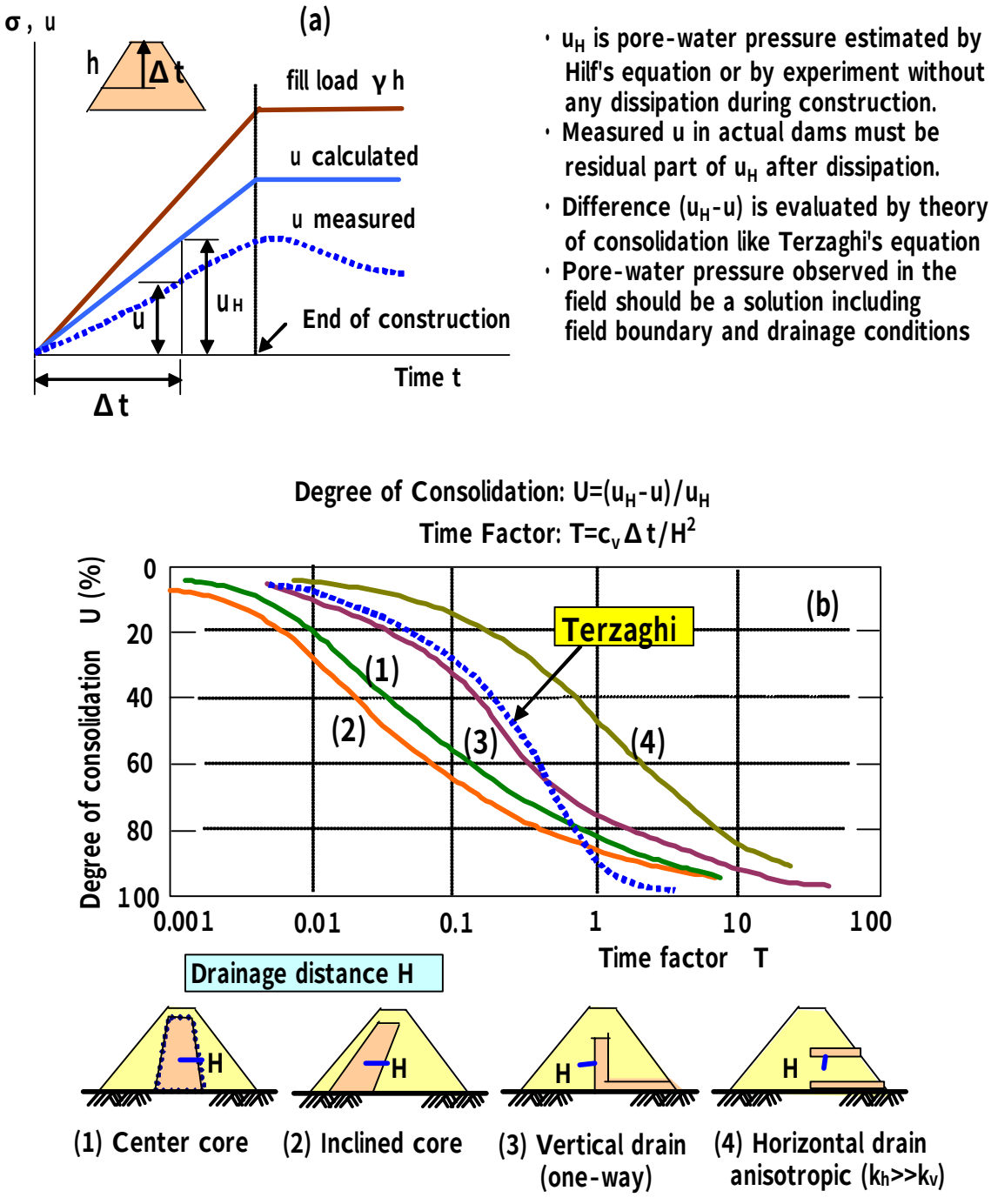

Fig.5.2 Dissipation of Pore-Water Pressure

5.3 Numerical Analysis of Pore-water Pressure in Embankments

The finite element method (FEM) has been one of useful tools in understanding stress and deformation behavior in embankment dams. Pore-water pressure developed in embankments during and after construction can also be evaluated well by FEM, as illustrated in Fig.5.3, by introducing a u-σ relation curve in estimating the built-up p.w.p., and one of U-T relation curves in Fig.5.2 in calculating dissipation of p.w.p. for corresponding dam type. Example calculation is demonstrated in Fig.5.4 for an earth dam of 30m high, showing a roughly good agreement between the observed and the calculated values of p.w.p..

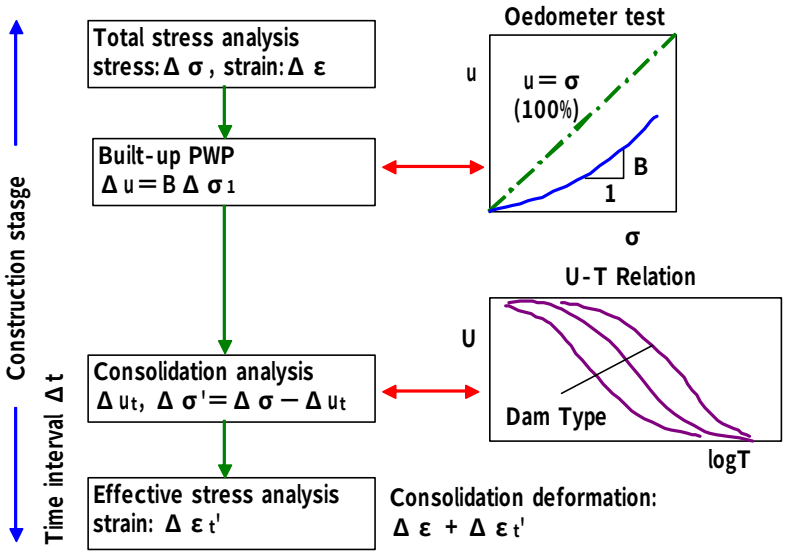

Fig.5.3
FE Analysis of p.w.p in Embankments

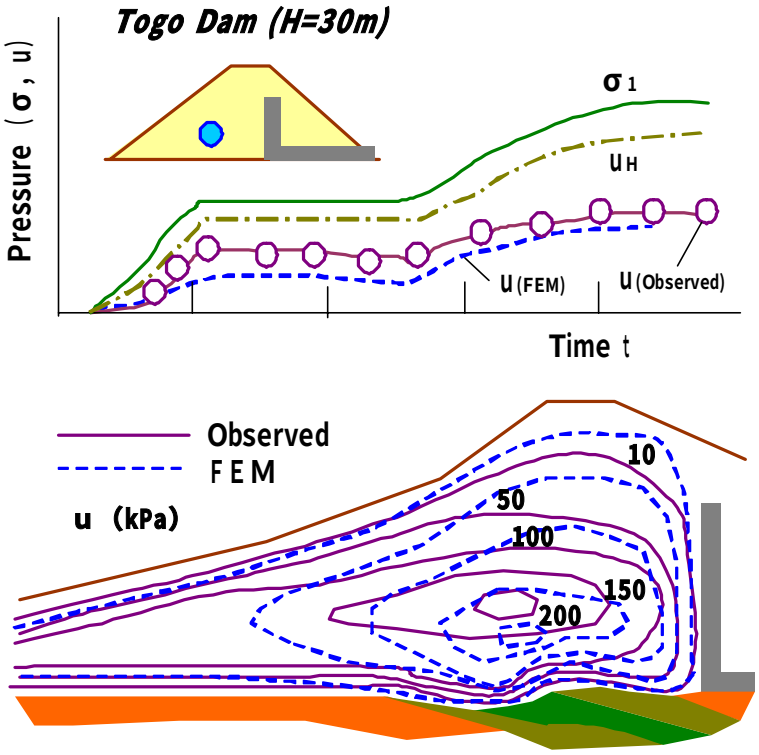

Fig.5.4 Estimation of p.w.p. in an Earth Dam

6. SEEPAGE THROUGH EMBANKMENT DAMS

6.1 Preface

The flow of water through void in soil can be described as a flow of water through a fine tube. It must be a laminar flow because the velocity of water through soil is comparatively low. The velocity beyond which the flow changes from a laminar flow to a turbulent flow is known as the critical velocity and it is related with Reynolds Number R_e expressed by

$$R_e = v_a D \frac{\gamma_w}{\mu g} \qquad \text{..... (6.1)}$$

where v_a is the velocity of water, D is the diameter of a tube, g is the acceleration of gravity and γ_w and μ are, respectively, the unit weight and the viscosity of water. The value of R_e corresponding to the critical velocity is given by 2.20.

Seepage problems usually encountered in geotechnical engineering deal almost exclusively with a laminar flow in which the equation of motion is expressed by the famous Darcy's law:

$$v_a = k \cdot i \qquad \text{..... (6.2)}$$

where k and i denote the coefficient of permeability and the hydraulic gradient, respectively. The range of R_e where Darcy's law is applied effectively is given by $R_e \leqq 1$.

6.2. Phreatic Surface in a homogeneous embankment

A.Casagrande proposed a procedure of estimating a phreatic surface to be formed within a homogeneous embankment. The procedure is illustrated for an example earth dam in Fig.6.1. It is assumed that the phreatic surface can be represented basically by a parabola with its focus point on the downstream toe of point A. The equation of this parabola is expressed by

$$x=(z^2-z_0^2)/2z_0, \quad z_0=(H^2+d^2)^{0.5}-d, \quad d=0.3l_1+l_2 \qquad \text{..... (6.3)}$$

where H is the depth of the reservoir. The basic parabola given by Eq.(6.3) somewhat differs from the actual phreatic surface on the upstream and downstream slopes. On the upstream side, the phreatic surface should intersect normal to the upstream face at a point B. The distance between the point B and the point B' where the parabola intersects the reservoir water level is assumed by $0.3l_1$. On the downstream side, the actual exit point C should lie somewhat lower than the point C' where the parabola intersects the downstream face. The distance Δa between the points C and C' can be determined from Eq.(6.4) and Fig.6.1.

$$a+\Delta a = z_0/(1-\cos\alpha) \qquad \text{..... (6.4)}$$

6.3. Phreatic Surface in an Inclined Core

A phreatic surface which must appear in an inclined core can be estimated easily by drawing as illustrated in Fig.6.2. Let us denote the width of the core at the water level as B' and that at the bottom as B. Plot the point D on the upstream face by taking a distance from the point P at the water level by (B'+B)/2 . Determine now the point Q on the lower face of the inclined core by drawing a circular arc PQ with its center at point D. The phreatic surface is then represented by the arc PQ.

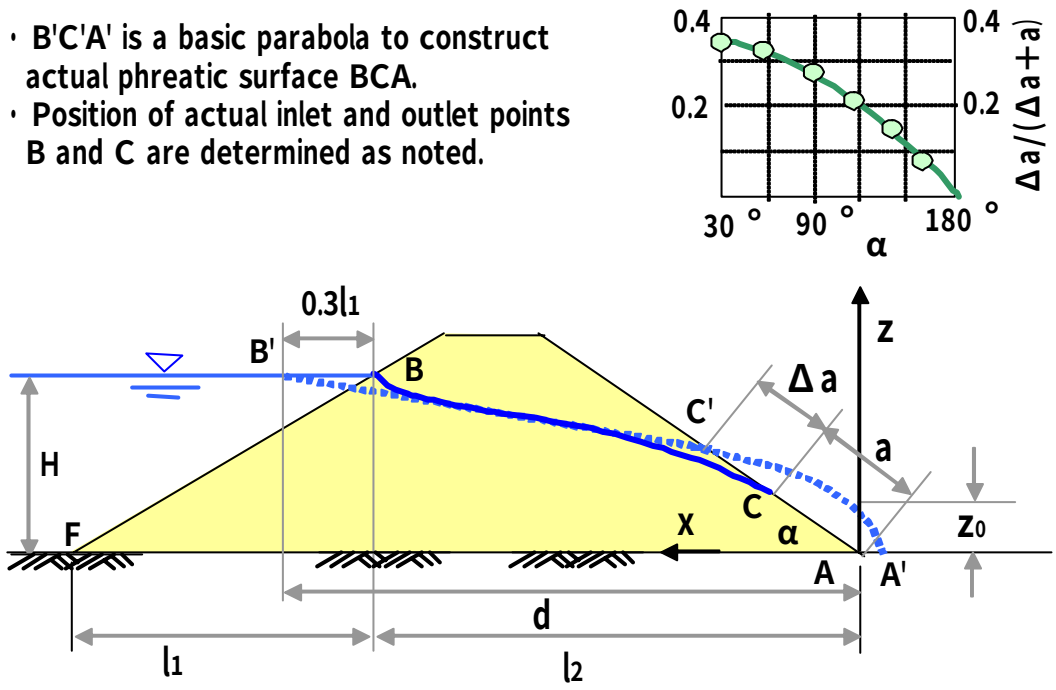

Fig.6.1 Phreatic Surface (Homogeneous Embankment)

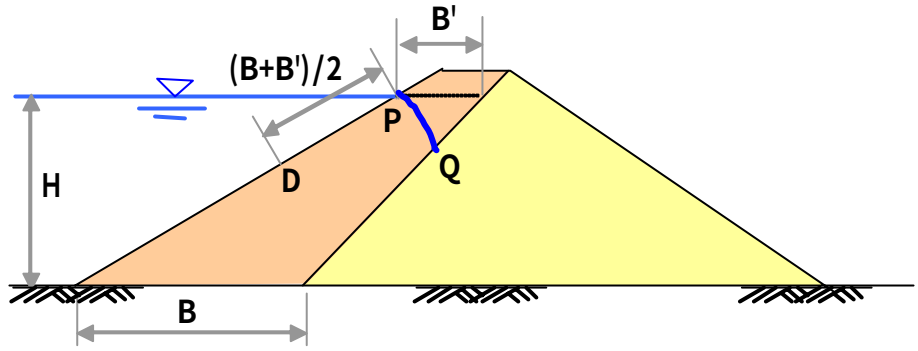

Fig.6.2 Phreatic Surface (Inclined Core)

6.4. Seepage Through Anisotropically Stratified Fills

It has often been pointed out that compacted fills are more or less stratified, having different permeability in the horizontal and vertical directions. The difference between the horizontal and vertical permeability, k_h and k_v, may vary to some extent according to the type of rollers used in the placement. It is known in general that the value of the ratio k_h/k_v ranges from 2 to 7, mean value of 5, in case of sheepsfoot roller compaction and from 10 to 40, mean value of 25, in case of that by a tired roller.

A well-known procedure to construct a flow net for such a stratified mass of soil is described in Fig.6.3. First of all, as an example in Fig.6.3(a), a typical flow net is drawn for a homogeneous and hydraulically isotropic earth dam ($k_h=k_v$). Flow net should be drawn to make square grids for

an isotropic medium. Suppose now an another earth dam of the same dimension which has different permeability in the horizontal and vertical directions ($k_h \neq k_v$). In order to draw a flow net for such a dam, the horizontal scale of the dam is first reduced by multiplying a scaling factor $(k_h/k_v)^{0.5}$ and a flow net is constructed assuming that the medium is isotropic. In Fig.6.3(b), a transformed section and a flow net thus drawn for the case $k_h=9k_v$ is presented. The true flow net is then obtained by increasing horizontal dimension of this reduced flow net, by multiplying $(k_h/k_v)^{0.5}=3$, as shown in Fig.6.3(c).

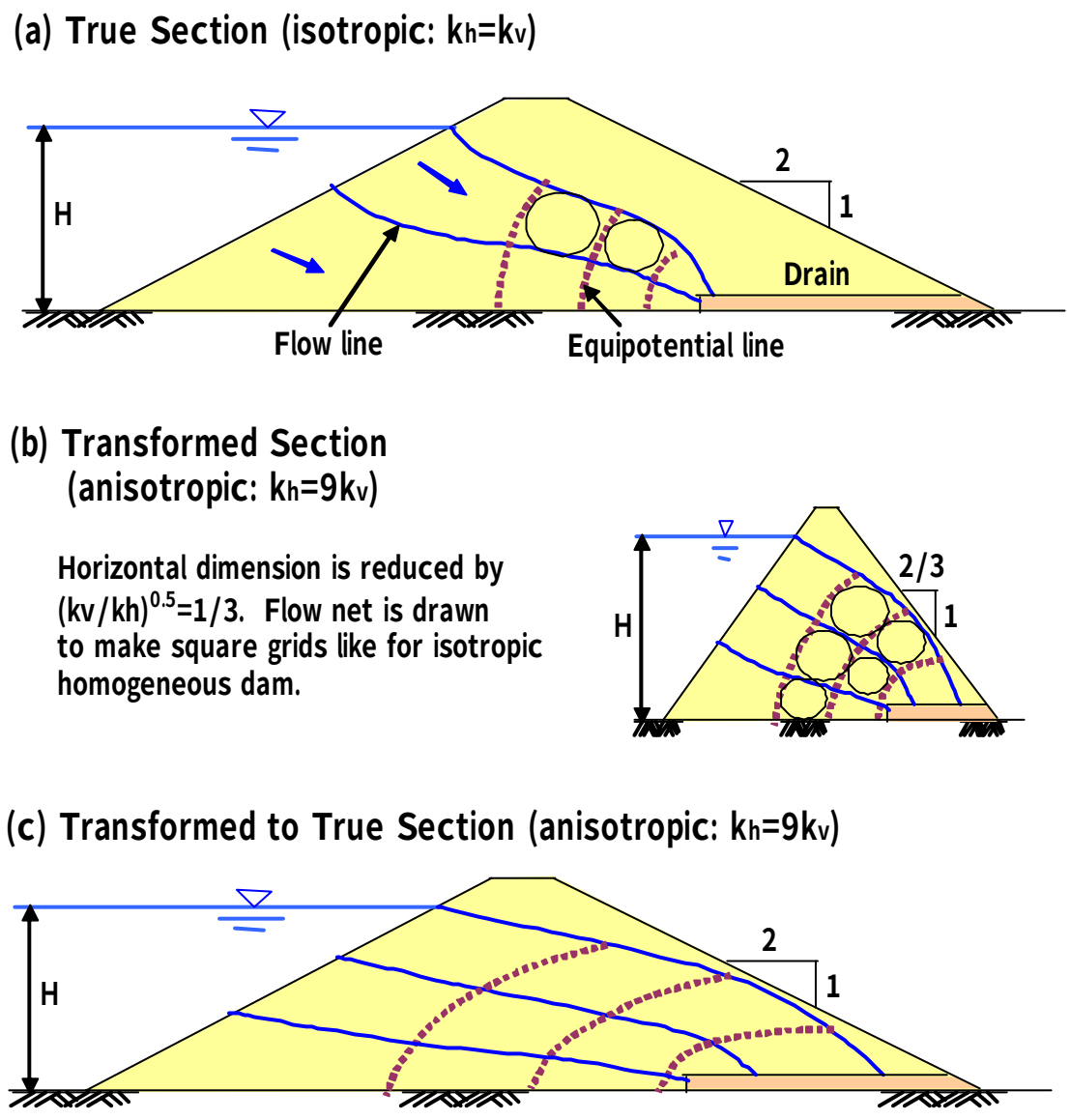

Fig.6.3 Seepage Through Anisotropic Embankment

7. SETTLEMENT AND CRACKING

7.1 Preface

Differential settlement and associated severe deformation such as open cracks, which develop in the interior and/or on the surface of embankment dams as shown in Fig.2.5, can be a direct cause of hydraulic fracturing, leading sometimes to a catastrophic damage and failure of fill bodies. In understanding the behavior of settlement and cracking in embankment dams, FEM is one of the most powerful analytical approaches for evaluating and studying the field behavior in actual dams.

7.2 Basic Concept of Settlement and Cracking

When a uniform load is applied on the surface of a soil foundation along a finite width, as illustrated in Fig.7.1, a saucer type settlement appears due to compression of the underlying soil layer. There are several points of interest in the relationship between the surface settlement and accompanied horizontal deformation, as follows: ①the horizontal displacement faces to the point of the maximum settlement and it becomes maximum at the steepest point of the settlement curve, where the horizontal strain vanishes, ②the horizontal strain is compression in the center zone of the settlement curve, and it is tension outside of it, and ③the horizontal strain becomes maximum at the steepest point of the horizontal displacement curve.

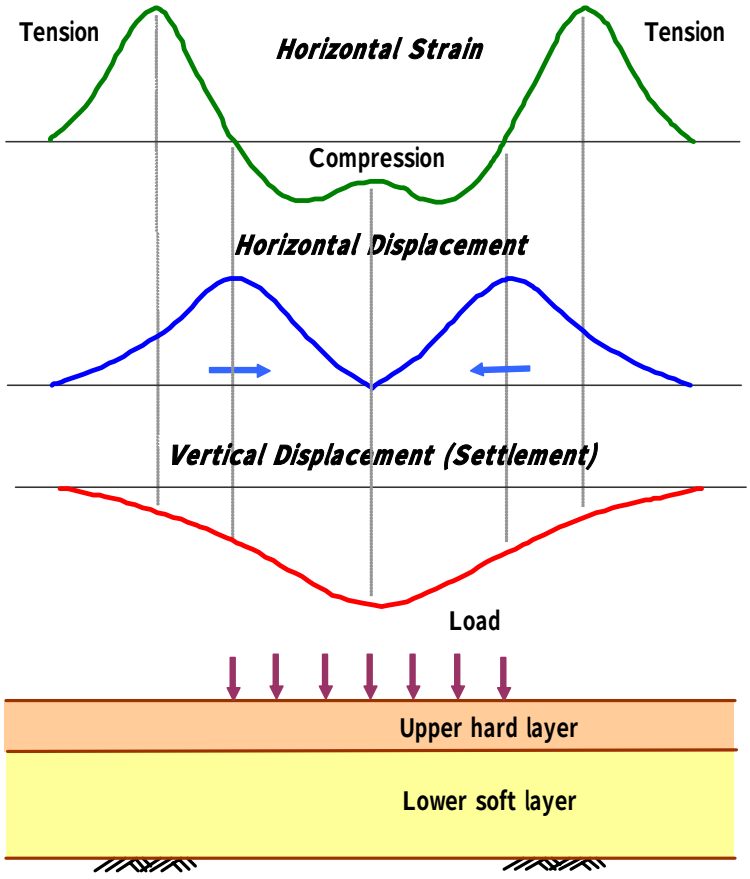

Fig.7.1 Relationship between Settlement and Horizontal Deformation

Similar characteristics of deformation are also pointed out in the F.E. solutions of gravity turn-on analysis on the longitudinal section of a homogeneous earth dam, as shown in Fig.7.2, where distributions of settlement and horizontal deformation are plotted along the crest surface of the dam. The settlement curve looks like a saucer, having the maximum value at the center of the valley. The horizontal displacement faces to the point of the maximum settlement, and it becomes to maximum at the steepest point of the settlement curve. The horizontal strain becomes tension outside the point of maximum displacement, and it becomes to maximum at the steepest point of the horizontal displacement curve.

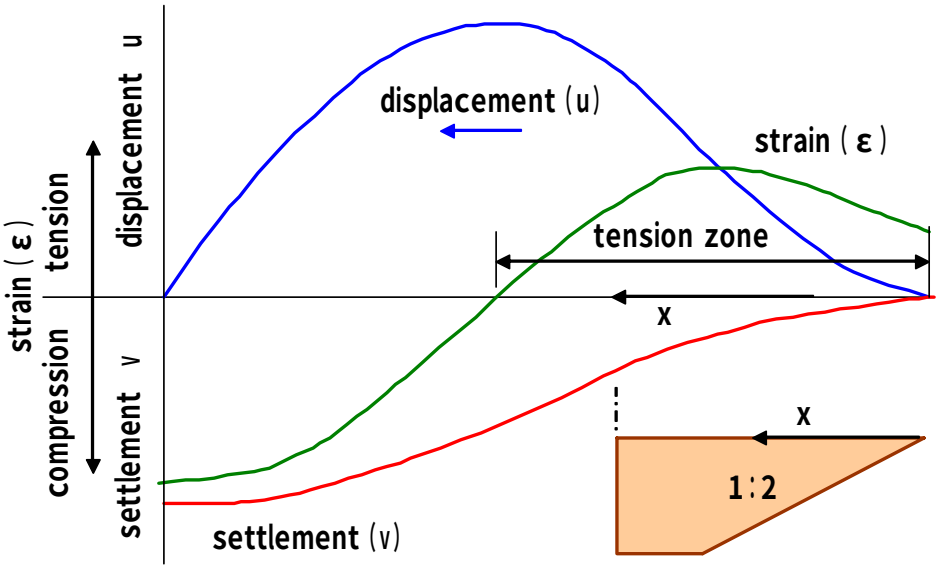

Fig.7.2 Distribution of deformation along crest

7.3 Field Behavior and Cracking Potential

The field behavior of settlement and cracking observed in a homogeneous earth dam is compared in Fig.7.3 with the F.E. elastic solutions of gravity turn-on analysis. The left part of the longitudinal section of the dam can be approximated by a simple trapezoid having a 1:1.5 slope and a horizontal base foundation, for which the F.E. solution of the left half of a fill of a symmetric trapezoid is effectively applied. The right part of the base foundation can similarly be approximated by a straight line of 1:2.0 slope, for which the F.E. solution of the right half of a V-shaped fill is the most applicable. It is recognized well in these figures that simple F.E. solutions are quite effective, quantitatively as well as qualitatively, in evaluating distributions of the settlement and the horizontal strain along the crest and cracking potential of the dam.

Field measurement and F.E. solutions on the relationship between the horizontal strain and the cracking potential along the crest of embankment dams are summarized in Fig.7.4. The measured and the calculated values of the maximum strain ε are normalized by a ratio of the settlement to the dam height w/H and plotted against slope inclination of the abutment (1:b). It is seen that the F.E. solutions roughly give the lower bound value of the measured strains at cracking and can be a useful material in estimating cracking potential in embankment dams.

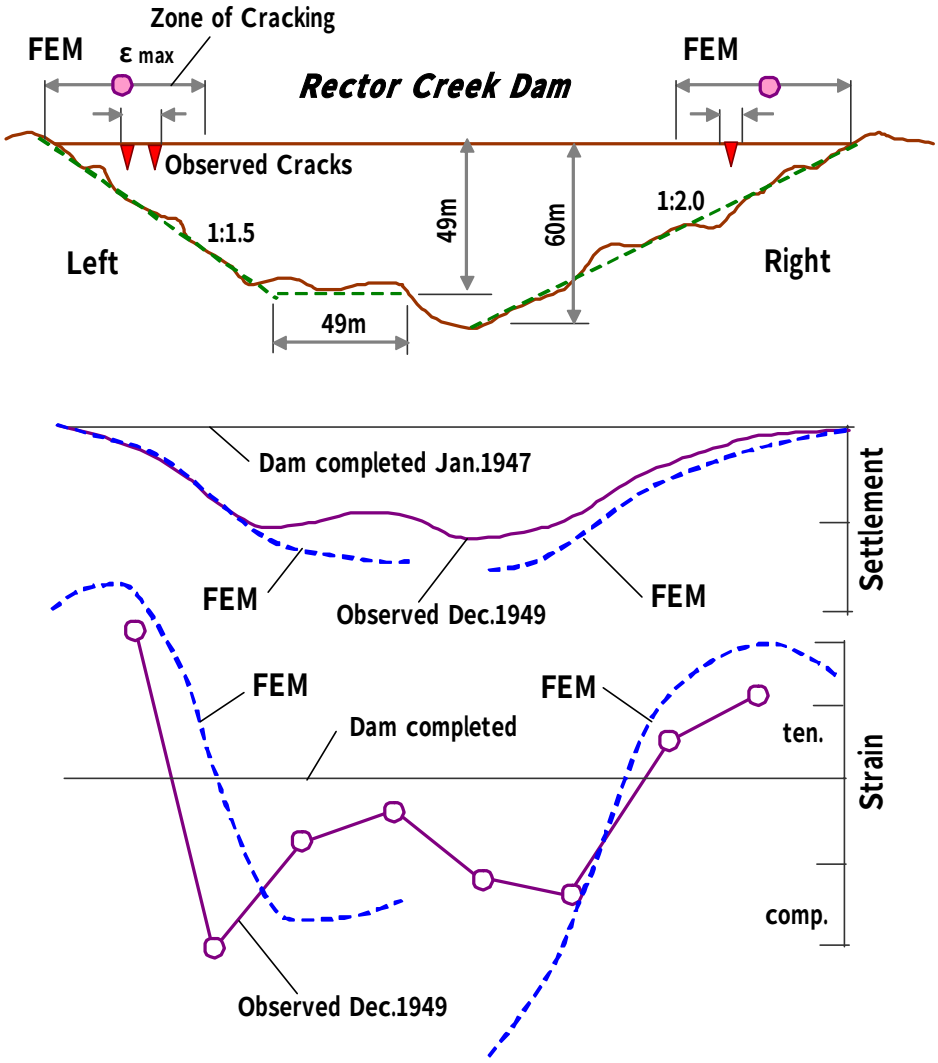

Fig.7.3 Comparison of deformation and cracking along crest

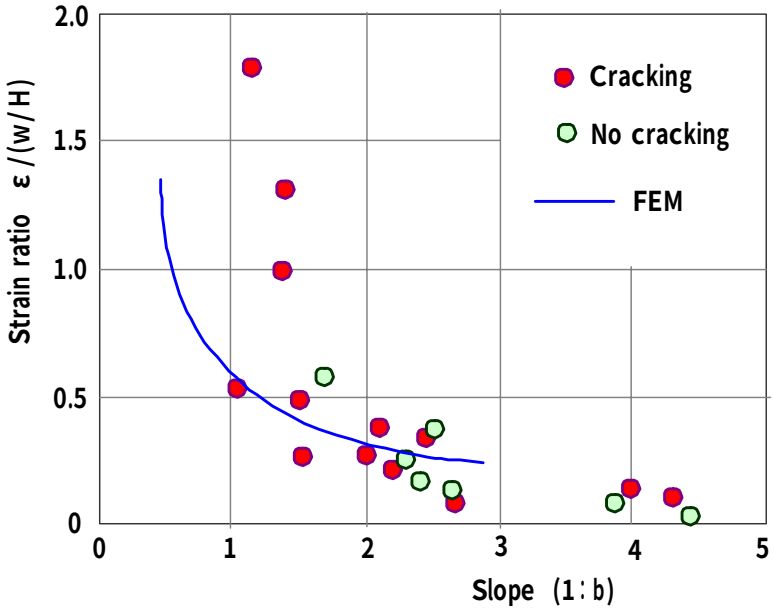

Fig.7.4 Cracking potential along crest

8. HYDRAULIC FRACTURING

8.1 Preface

In recent years, hydraulic fracturing has been a matter of great concern in the design and construction of embankment dams. Extensive studies have been done on this subject especially since the failure of Teton Dam (USA) in 1976.

Hydraulic fracturing can be considered equivalent to the well-known seepage failures such as quick sand and piping. One of typical examples of hydraulic fracturing, which engineers can understand easily in the first step, must be a fracture of ground during field permeability test, as described in Fig.8.1. The permeability measured at a high water pressure head becomes excessively large due to hydraulic fracture in the ground as compared with the one measured at a small head. It should be noted that the water pressure beyond which hydraulic fracture occurs is sensitive to the stress state at the site and comparatively lower than the effective overburden pressure at that point.

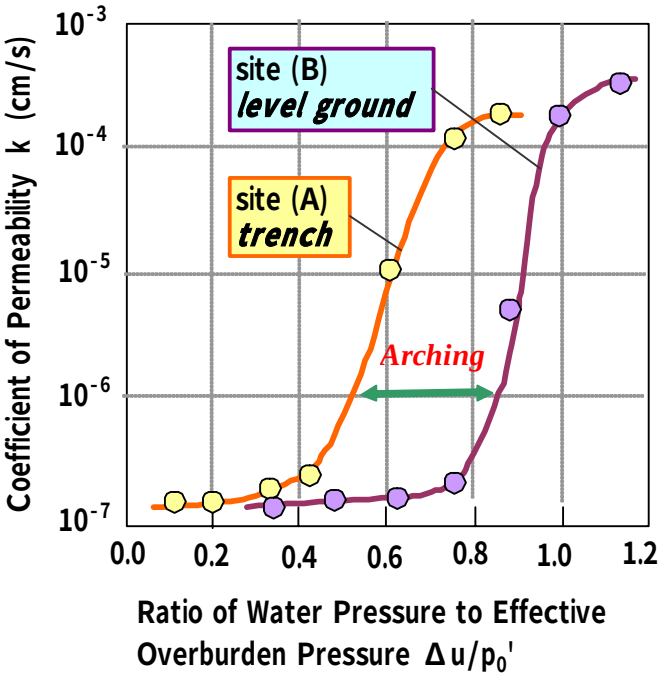

Field Permeability Test

- The permeability of unfractured clay tested at small head Δu is of the order of $1\text{-}2\times10^{-7}$cm/s, but this increased sharply when testing pressure exceeded $0.4\text{-}0.5p_0'$ at site (A) and about $0.8p_0'$ at site (B).
- Very low failure pressure at site (A) is considered to be due to "arching", where weight of overburden was carried to a large extent by shear stresses along wall of trench.
- Fracture usually takes place at about $0.8p_0'$, less than overburden pressure, like at site (B) even though arching is eliminated, which demonstrates that critical pressure against hydraulic fracturing must be horizontal stress or minor principal stress.

Fig.8.1 Hydraulic Fracture During Field Permeability Test

8.2 Hydraulic Fracture in Fill-type Dams

The mechanism of hydraulic fracture observed in embankment dams is not so simple because configuration and interaction of the embankment and surrounding abutment foundation are very complicated. Fracture generally occurs when a state of zero effective stress appears near the interface of the core zone and the abutment foundation in accordance with the progress of differential settlement in embankment, in which soil materials are washed away from the core zone by erosion and it leads to progressive erosion and piping.

Two distinct patterns of hydraulic fracturing can be considered in embankment dams. One is the case where differential settlement after construction is contributive to cause cracking in the embankment and erosion takes place due to the flow of the reservoir water passing through open cracks. When embankment deformation is accompanied by differential settlement, tensile strains develop on the surface or in the interior of the embankment, and the minor principal stress σ_3 tends to decrease locally to open tension cracks. The criterion for the possibility of hydraulic fracturing in this case is represented by the condition:

$$\sigma_3 < -p_t \qquad \text{.....(8.1)}$$

in which p_t is the tensile strength in terms of total stress. Corresponding stress state is indicated in Fig.8.2(a), where the initial stress circle (Ⅰ) grows on the left side due to the decrease in σ_3 and touches the failure envelop at the circle (Ⅱ) to open tension cracks.

The other pattern is the case where pore-water pressure in the core increases according as the reservoir filling proceeds and the effective stress σ_3' decreases up to the effective tensile strength p_t' to open unseen or latent cracks. The criterion in this case is given by

$$\sigma_3' < -p_t' \qquad \text{.....(8.2)}$$

and stress states are illustrated in Fig.8.2(b), where the initial stress circle (Ⅰ) shift to the left without diameter change and touches the envelop at the circle (Ⅱ).

The criterion is summarized when $p_t=p_t'$, in place of Eqs.(8.1) and (8.2), in the following form:

$$\sigma_3 + p_t < p_w \qquad \text{.....(8.3)}$$

in which p_w is the hydrostatic pressure. Eq.(8.3) reduces to Eq.(8.1) when $p_w=0$, that is, when p_w should not be taken into account before impounding.

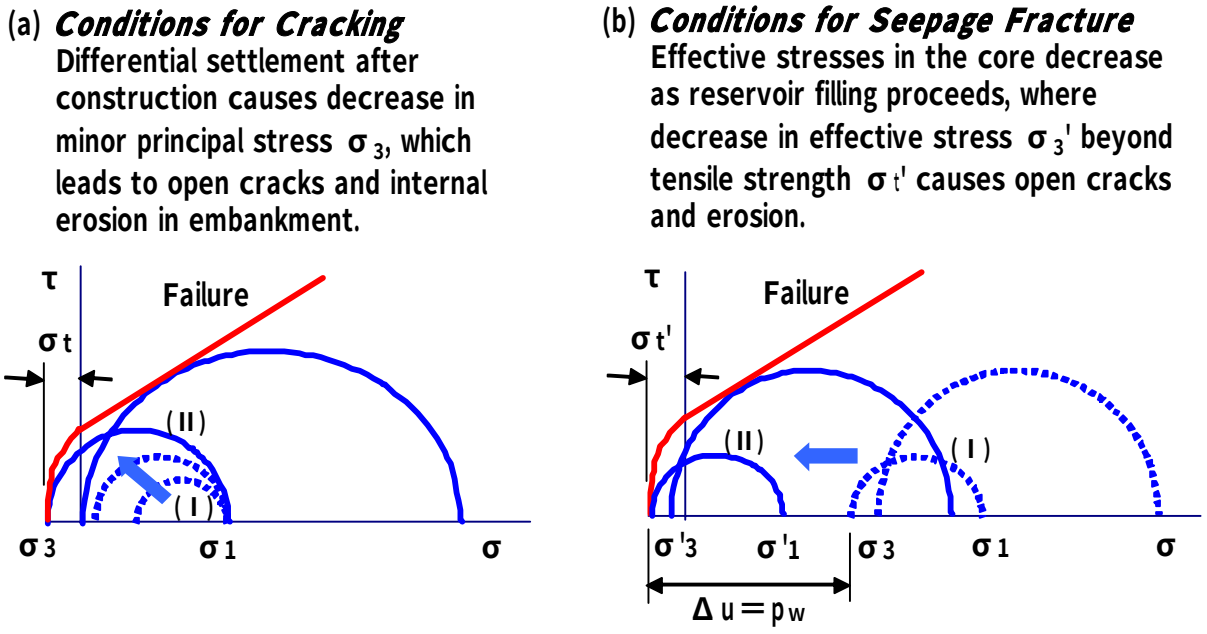

Fig.8.2 Hydraulic Fracturing in Embankment Dams

Two typical patterns of hydraulic fracturing, which engineers often encounter in the field, are again illustrated in Figs.8.3 and 8.4.

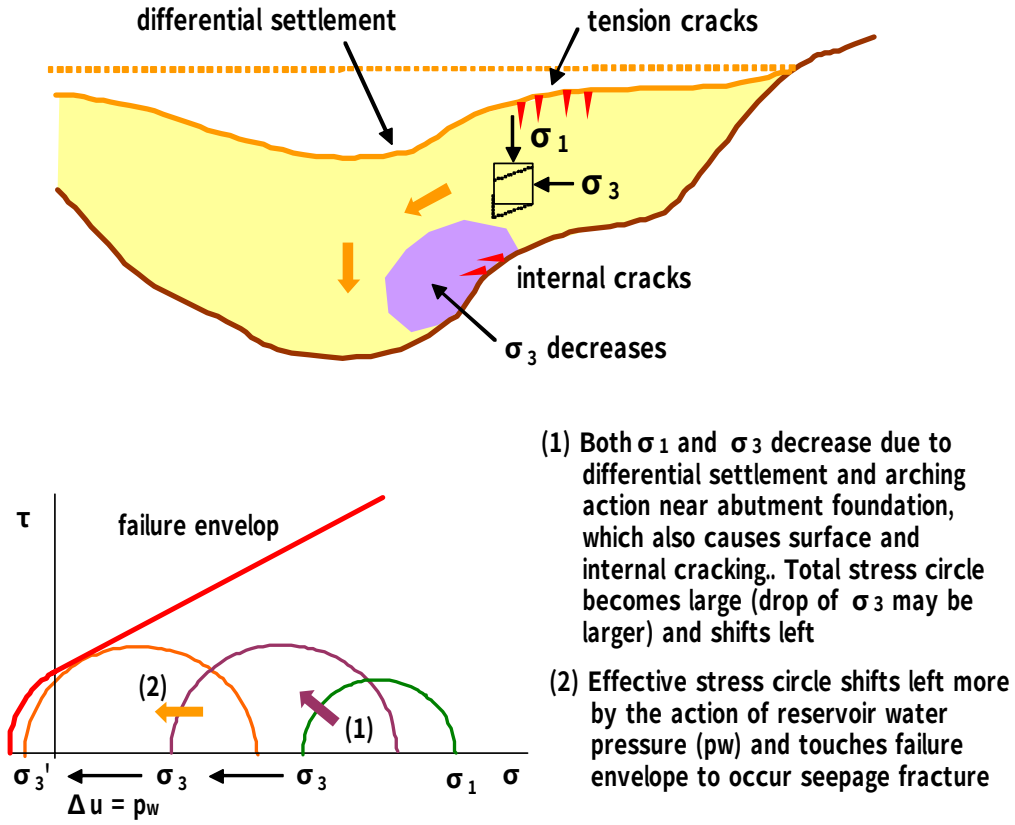

Fig.8.3 Hydraulic Fracturing Type (1): Differential Settlement and Cracking

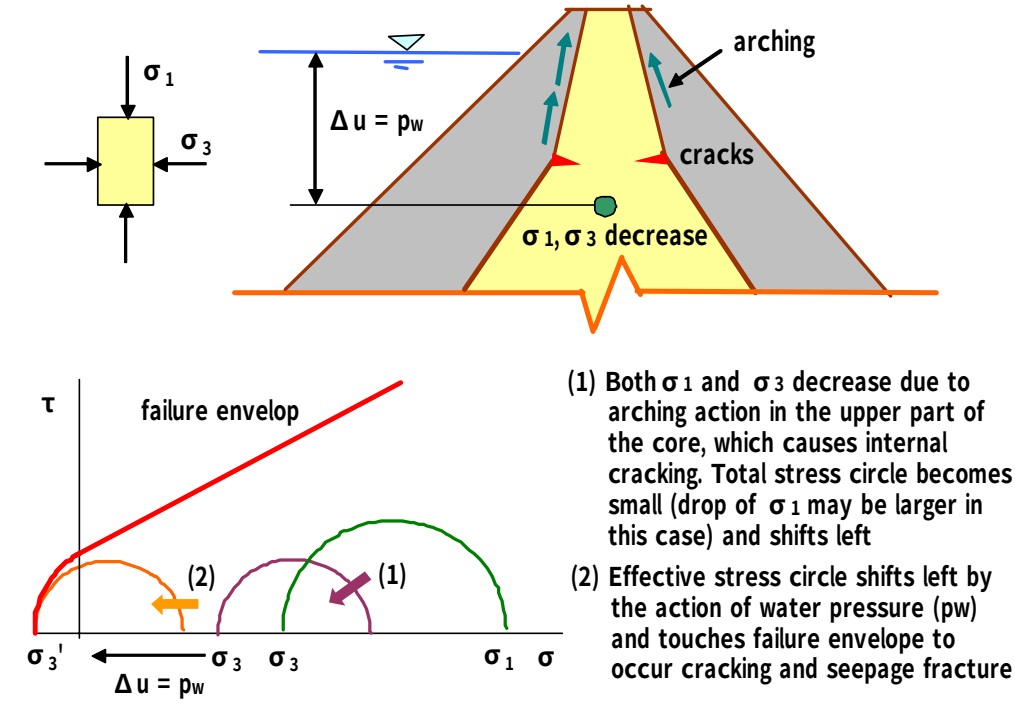

Fig.8.4 Hydraulic Fracturing Type (2): Cracking and Seepage

9. EARTHQUAKE RESISTANT DESIGN OF EMBANKMENT DAMS

9.1 Preface

It has not yet been reported so far that large earth and rockfill dams have experienced serious damages including sliding failures to cause severe economic and social losses, though they have often been attacked by strong earthquakes of the maximum acceleration far beyond the design value. In the Naganoken-Seibu earthquake in 1984 (Japan, M=6.8), for instance, the epicenter was several hundred meters far from Makio dam, a centrally located core type rockfill dam of 105m in height, and the maximum acceleration at the crest of the dam was estimated to be almost the same as the acceleration of gravity (g=980gals). In the Morgan Hill earthquake in 1984 (USA, M=6.2), the maximum acceleration observed at the left side abutment foundation of Coyote dam site was as large as 1.29 times of g. Serious damages, however, were not reported in these cases except for small open cracks on the crest and/or shallow slip of rockfill slopes even though the embankments were under such strong excitation of more than several times as large as the design value of acceleration. This is to be said due to an essential shortcomings of the ordinary seismic coefficient method (SCM) in which dynamic forces developed in an embankment during earthquake are treated statically by introducing the equivalent seismic inertia forces distributed uniformly from bottom to crest.

In Fig.9.1, a little cracking damages observed on the crest of La Villita dam (Mexico, H=60m) caused by the 1985 Mexico Earthquake (M=8.1) is illustrated as an example. In this earthquake, the acceleration observed at the crest reached up to about 0.7g, but only two lines of cracks of about 50cm deep were detected along the axis of the dam.

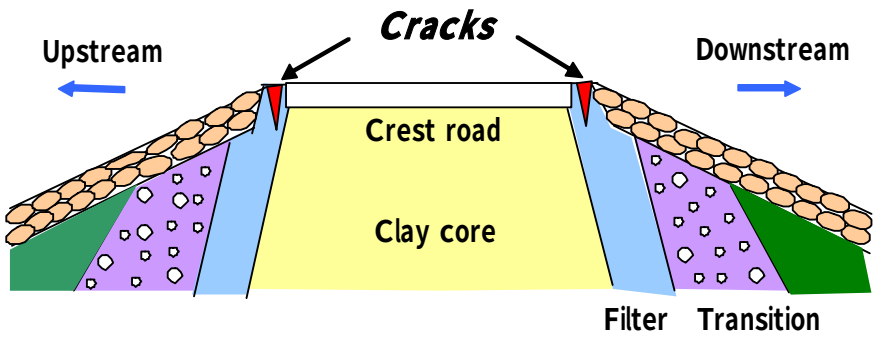

Fig.9.1 Damage Caused by Mexico Earthquake in 1985 (La Villita Dam)

9.2 Japanese Standard of Earthquake Resistant Design

It is generally known that when an embankment resting on foundation is subjected to an earthquake excitation, the acceleration response at the crest becomes considerably high as compared with the input acceleration at the base. In this case, sliding failures likely take place in the crest part because of seismic instability. Fig.9.2 shows the relation between the base acceleration and the response acceleration at the crest observed in actual dams and in laboratory shaking table tests. Because of the non-linear dynamic deformation properties of fill materials, the acceleration ratio of α_t to α_B decreases as the intensity of the base acceleration α_B increases.

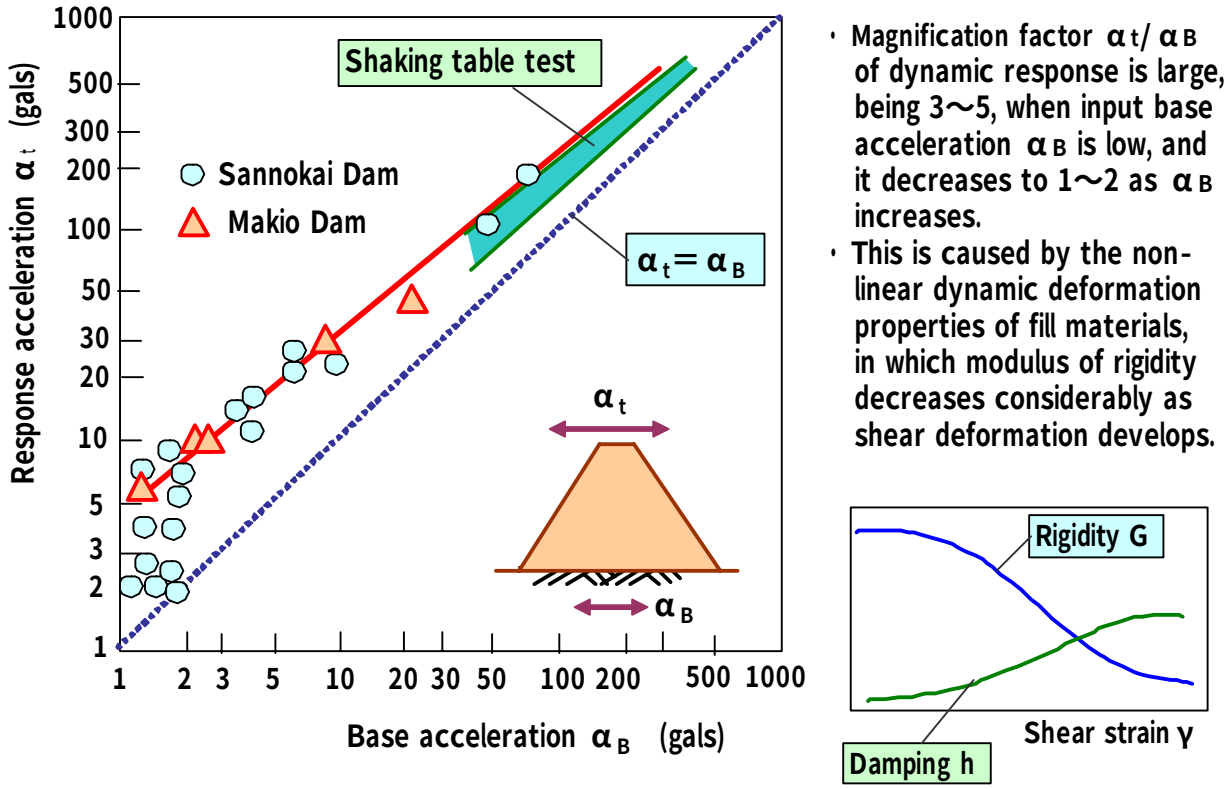

Fig.9.2 Magnification Factor of Dynamic Response

Through extensive studies on the dynamic response of earth and rockfill dams, laboratory shaking table tests on model fills, element tests on fill materials, analysis of observation data in the field and FEM dynamic response analysis, a modified and advanced method of SCM (the Japanese Standard Method) of earthquake resistant design was proposed in 1991, as presented in Fig.9.3. One of points to be noted is that a bi-linear distribution of seismic coefficient is adopted to consider actual behavior of dynamic response of embankment. The parameter k_F is the design seismic coefficient at the base foundation, which taking local seismicity into account can be changed higher and lower in accordance with the location of dam site. In Japan, the value of k_F is taken as 0.13 (low level area) to 0.18 (high level area), as shown in Fig.9.4.

REFERENCES

1) Yamaguchi,H. and Ohne,Y.: "Design and construction of fill dams," Giho-do, 1973.
2) Sherard,J.L, et al.: "Earth and earth-rock dams," John Wiley & Sons, 1963.
3) Ohne,Y. and Narita,K.: "Discussion on cracking and hydraulic fracturing in fill-type dams," Speciality session 8, 9th ICSMFE, 1977.
4) Narita,K. and Ohne,Y.:"A simplified method of estimating construction pore pressure in earth dams," S & F, 23-4, 1983.
5) Narita,K. and Ohne,Y.:"A study on crack generation in fill-type dams," S & F, 18-1, 1978.
6) Ohne,Y. et al.: "The study on the vibration properties of fill dams," 12th ICOLD, 1976.
7) Ministry of Construction: "A proposal to the seismic resistant design of fill dams," 1991.

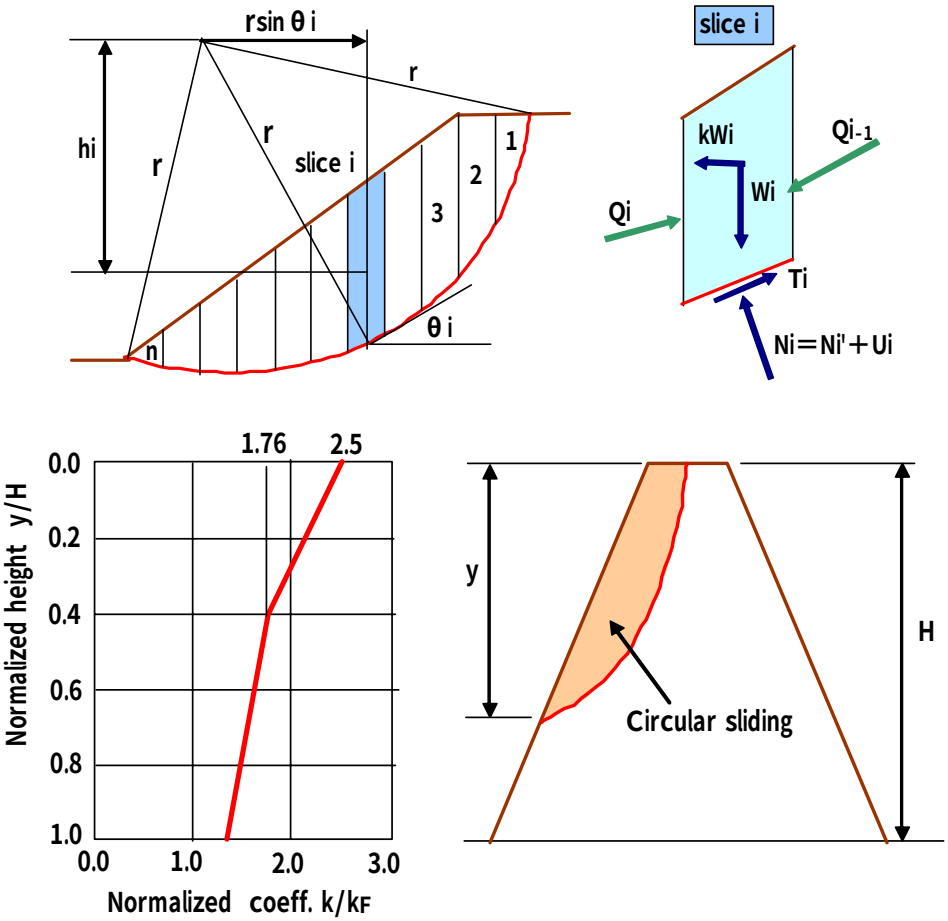

Fig.9.3 Japanese Standard Method of Earthquale Resistant Design

Fig.9.4
Local Design
Seismicity in Japan